

CURRICULAR ACADEMIC INTERNSHIPS  
ASTRONOMICAL OBSERVATORY

# INTRODUCTION TO OBSERVATIONAL SPECTROSCOPY

Ángela Abad Martín

Professional Supervisors: Ángeles I. Díaz Beltrán, Asier Castrillo Varona,  
Sandra Zamora Arenal

Academic Supervisor: Violeta González Pérez

2022/2023 Academic Year

## Summary

Observational astronomy allows, through the exploration of celestial bodies, to study their characteristics and peculiarities by means of telescopes, other astronomical instruments and the use of digital programs.

During the elaboration of this project, the main objective was to formulate computational codes via Python in order to analyze the data belonging to astronomical objects of interest such as nebulae and stars, particularizing the study of the Orion Nebula and the Ring Nebula, with two calibration stars each (Rigel and Betelgeuse for Orion and Sulafat and HD-176896 for the Ring). The data with which we work below were collected during the observation carried out on November 10 at the Astronomical Observatory of the Autonomous University of Madrid. We begin by reducing the raw data obtained to later calibrate the flux and wavelength of the spectra of the stars selected for each nebula in order to generate the instrumental response curve associated with the electronic device used. From this, the spectra of the final nebulae are determined. With the latter, and eliminating the continuous contribution to the spectrum, the characteristic lines of each nebula are finally obtained, which represents an initiation into the technique of observational spectroscopy of celestial bodies.

# **Index**

1. Introduction .....	1
2. Code development and discussion of results .....	2
2.1. Developing the data reduction code.....	2
2.1.1. Master Bias.....	3
2.1.2. Master Dark.....	3
2.1.3. Master Flat.....	4
2.2. Spectral analysis of mercury and neon lamps.....	4
2.3. Applying corrections for data reduction .....	5
2.3.1. Profit analysis .....	5
2.3.2. Image reduction, rotation and cropping.....	5
2.4. Wavelength calibration of stellar spectra and subtraction of the sky contribution.....	6
2.5. Flux calibration of stellar spectra and instrumental response curve.....	8
2.6. Calibration to nebula wavelengths and subtraction of sky contribution.....	10
2.6.1. Orion Nebula .....	11
2.6.2. Ring Nebula.....	11
2.7. Generation of nebula spectra from the instrumental response curve.....	12
2.8. Continuum removal and representation of the final spectra of nebulae ....	13
3. Conclusions .....	15
4. References .....	16

# 1. Introduction

The field of astronomical spectroscopy allows us to characterize the physical-chemical qualities of celestial bodies through the study of their electromagnetic spectra, that is, their type of radiation. In these, a series of properties are usually observed, such as spectral lines (within which emission and absorption lines are distinguished depending on whether the peaks are increases in radiation intensity or decreases, respectively) and a continuous contribution, which may present discontinuities throughout the entire spectrum.<sup>[1]</sup>.

During the project, the spectra of stars and nebulae are observed and analyzed with the aim of determining the characteristic lines corresponding to the latter and thus being able to compare the differences between different astronomical bodies. It should be noted that, before developing the detailed study below, we began by treating images and data recorded from previous astronomical observations (carried out by students of the Master's course at the Autonomous University of Madrid, TOA) with the aim of establishing familiarity with the programs to be used (Python) and with the study techniques, neither of which had been previously treated. However, the final observation work carried out is detailed below.

Throughout the planning of the observation, the main objective was to analyze four nebulae, each with two associated calibration stars (one blue and one red) in order to develop the instrumental response curve detailed later in section 2.5. However, due to a miscalibration of the digital program that contributed to a delay not previously contemplated during the planning, it became impossible to measure two of the nebulae that were already outside the field of view by then. Also, although not as decisive, the weather (clouds) had an influence, a difficulty that could be solved by organizing the observation in such a way that the most visible astronomical bodies were measured first before those behind the clouds. In this way, the following were mainly analyzed:

- Orion Nebula (NGC 1976): Rigel (blue) and Betelgeuse (red).
- Ring Nebula (NGC 6720): Sulafat (blue) and HD-176896 (red).

It is worth noting that additional astronomical bodies such as Vega, IOTA Aquarii, 88 Aquarii and the Moon were observed despite not being analyzed during the study. In addition, mercury (Hg) and neon (Ne) spectral lamps were measured in order to determine the width of the slit used, the rotation angle of the images and the calibration of pixels to wavelengths, all of which are detailed in sections 2.2 and 2.3.

## **2. Code development and discussion of results**

The main steps carried out during the development of the computational code are detailed below, reviewing the most determining points and the characteristic results obtained.

### **2.1. Developing data reduction code**

Throughout the process of observing astronomical bodies, a series of raw data are collected, in which the presence of background noise must be considered, which is subsequently suppressed with data reduction techniques. Essentially, there are three types of noise: reading noise ("Bias"), thermal noise ("Dark") and noise from the optics and sensors of the instrument ("Flat").

When photons with sufficient energy reach the telescope's CCD (light detector based on semiconductor materials), they can excite and store electrons in the sensor's pixels. A voltage signal counts the number of electrons stored in each pixel and once each cell has been counted, it is "erased" and all the electrons are moved to the adjacent cell to continue counting. In reality, however, some electrons may be left behind during movement, causing a trail in the image that would not necessarily belong to the morphology of the observed body. These errors are called "Bias". These are images that only contain reading noise, so they are taken at zero exposure time and with the telescope covered to read only the CCD.

Sometimes it happens that due to the wiring and the electric currents that flow under the CCD, electron excitations occur due to thermal effect, which causes an excess of counts in the pixels, an effect that is usually seen as a background noise that increases as the temperature increases and that prolongs with the telescope's exposure time; this is the "Dark". They are measured with the telescope covered and a non-zero exposure time and as close as possible to the measurement of the astronomical body that we have studied.

Finally, there is the "Flat" noise, which comes from the inhomogeneities of the lenses and the uneven illumination created by dust or spots in the optical train and is closely related to the quantum efficiency of the sensor. It is reflected as a vignetting in the corners or as "donut" shaped spots. There are several types of "Flats": dome noise (the dome is closed and a cloth is illuminated as homogeneously as possible), sky noise (images are taken of a "practically" homogeneous area of the sky, having to take measurements at dusk or dawn) and bulb noise (in the dark the telescope is pointed directly at an incandescent light bulb; method used during observation). "Flats" files are measured with a non-zero exposure time and with the telescope open.

We start by developing a code that allows, from a collection of “Bias”, “Darks” and “Flats”, to develop “Master Bias”, “Master Darks” and “Master Flat” that will be applied for data reduction later on.

### 2.1.1. Master Bias

Below are the steps to follow during the preparation of the “Master Bias” (see *Figure 1*). To do this, 10 “Bias” frames were measured with a temperature of  $-10^{\circ}$  and a gain of 140.

*Figure 1.* “Master Bias” code.

```

1 Direccion_Carpeta_Bias = 'BIAS/17_37_36/*.fits' # Dirección de la carpeta "BIAS" (solo los archivos .fits)
2 Lista_Bias = glob.glob(Direccion_Carpeta_Bias) # Genera una lista de todos los archivos .fits de la carpeta "BIAS"

1 # Se genera un array 3D donde se pueda meter cada archivo .fits en forma de capas. Para ello el array debe tener
2 # las dimensiones (z,y,x):
3 # - Primera variable (eje "z"): se trata de cada una de las capas (por ello se indica "len(Lista_Bias")).
4 # - El resto de dimensiones (ejes "y" y "x"): deberían ser siempre las que salgan por defecto al abrir un archivo
5 # Bias cualquiera usando la función hdu.info(). Sale:
6 # NAXIS1 = 4656 (este es nuestro eje "x").
7 # NAXIS2 = 3520 (este es nuestro eje "y").
8
9 A = np.zeros((len(Lista_Bias),3520,4656)) # Array vacío que se llena a continuación.
10
11 for i in np.arange(len(Lista_Bias)):
12     hdu = fits.open(Lista_Bias[i]) # De la "Lista_Bias" se van sacando uno por uno cada archivo Bias ".fits"
13     A[i] = hdu[0].data # y se van metiendo en la variable A, creando así cada capa.

1 # Se realiza el promedio sobre todas las capas para así poder crear el "Master Bias". Se aplica la función
2 # np.nanmean en lugar de np.mean para así evitar arrastrar posibles valores "not a number" en el proceso:
3
4 MASTERBIAS = np.nanmean(A,axis = 0) # Promedio de todos los Bias en el eje 0 (eje de las capas = eje z).
5
6 # Se crea un archivo .fits en nuestro entorno de python con nombre MB (de Master Bias) que contendrá los
7 # datos del MASTERBIAS calculados recientemente. Se guarda en la carpeta de "MASTERS", ya creada:
8
9 MB = fits.PrimaryHDU(MASTERBIAS)
10 MB.writeto('MASTERS/MasterBias.fits')
```

### 2.1.2. Master Dark

To prepare the “Master Dark” we proceed in a similar way to section 2.1.1., only this time taking into account the distinction of measurements based on the exposure times used. We measured 10 “Darks” of 2, 20, 40 and 60 seconds, all of them with a gain of 140 and maintaining the temperature around  $-10.5^{\circ}$ . Likewise, a peculiarity is highlighted and that is that for these measurements the contribution of the “Master Bias” has to be eliminated since it is always present during data collection (see *Figure 2*).

*Figure 2.* Final section of the code “Master Dark” for different exposure times.

```

1 # Se crean los Master Dark "con ruido" para cada tiempo de exposición:
2
3 MASTERDARK_2_RUIDO = np.nanmean(t_2,axis = 0)
4 MASTERDARK_20_RUIDO = np.nanmean(t_20,axis = 0)
5 MASTERDARK_40_RUIDO = np.nanmean(t_40,axis = 0)
6 MASTERDARK_1_RUIDO = np.nanmean(t_1,axis = 0)
7
8 # Finalmente se obtienen los Master Dark "sin ruido" para cada tiempo de exposición, eliminando para cada uno de
9 # ellos el Master Bias generado anteriormente:
10
11 path_MasterBias = 'MASTERS/MasterBias.fits'
12 MasterBias = fits.open(path_MasterBias)
13
14 MASTERDARK_2 = MASTERDARK_2_RUIDO - MasterBias[0].data
15 MASTERDARK_20 = MASTERDARK_20_RUIDO - MasterBias[0].data
16 MASTERDARK_40 = MASTERDARK_40_RUIDO - MasterBias[0].data
17 MASTERDARK_1 = MASTERDARK_1_RUIDO - MasterBias[0].data
```

### 2.1.3. Master Flat

We finish by carrying out the same process described above for a string of 10 bulb “*Flats*” for an exposure time of approximately 1.43 seconds, gain of 140 and temperature of  $-9.5^{\circ}$ . In this case, there are two other peculiarities to take into account: firstly, both the “*Master Bias*” and the “*Master Dark*” corresponding to the selected exposure time are subtracted. For this specific case, due to the fact that “*Darks*” with exposure times less than 2 seconds are presented, the following operation is performed:

$$\frac{\text{Master Dark } (x \text{ segundos})}{x \text{ segundos}} = \frac{\text{Master Dark } (y \text{ segundos})}{y \text{ segundos}} = \dots \quad (1)$$

assuming  $x = 2s$  and  $y = 1.43s$ . On the other hand, the string of corrected “*Flats*” needs to be normalized before performing the “*Master*” in order to rescale the results obtained and thus obtain the same value for the pixels with greater luminosity<sup>[2]</sup> (in addition to the fact that this procedure eliminates the time units from the “*Master Flat*”) (see *Figure 3*).

**Figure 3.** Fragments of the peculiarities to be considered during the elaboration of the “*Master Flat*”

```

21 for i in np.arange(len(Lista_Flats_bomb)): # RECORDEMOS QUE "Flats_cielo" TENÍAN texp=1,425785s
22 hdu_bruto_bomb = fits.open(Lista_Flats_bomb[i])
23 corregido_bomb = hdu_bruto_bomb[0].data - MasterBias[0].data - (MasterDark_2s[0].data * 0.7128925)
24 Flats_bomb_corregidos[i] = corregido_bomb # Array de Flats_cielo "sin ruido"

8 media_flats_bomb = np.nanmean(Flats_bomb_corregidos, axis = (1,2)) # Media de cada Flat del Flats_corregidos
9 # (se hace la media en las direcciones "y"
10 # y "x", es decir, en cada capa por separado).

19 Flats_bomb_ready = np.zeros((len(Lista_Flats_bomb), 3520, 4656))
20
21 for i in np.arange(len(Lista_Flats_bomb)):
22     Flats_bomb_ready[i] = Flats_bomb_corregidos[i] / media_flats_bomb[i] # Array de Flats_bomb corregidos y
23     # normalizados

```

## 2.2. Spectral analysis of mercury and neon lamps

The spectra belonging to mercury and neon lamps allow, first of all, to determine the position of the emission lines of each element in order to establish the relationship of pixels to wavelengths using a calibration guide.<sup>[3]</sup>.

**Figure 4.** Spectra of Hg and Ne lamps.

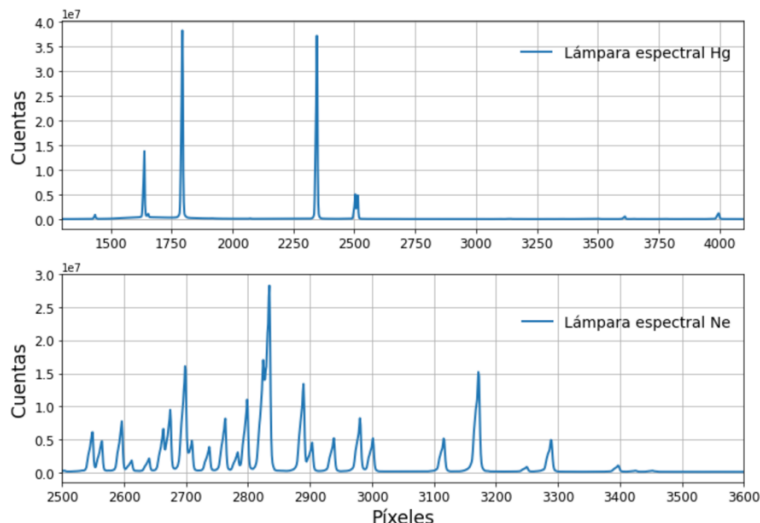
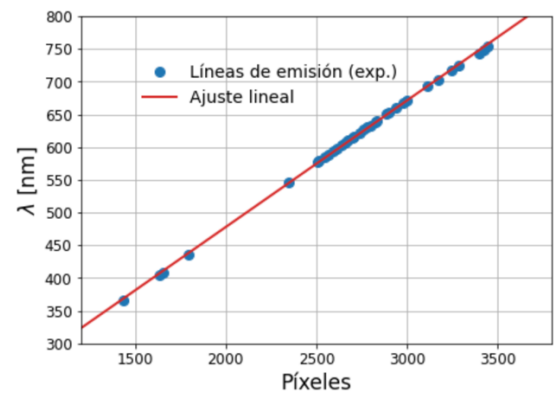


**Figure 5.** Calibration to wavelengths.



In *Figure 5* a linear fit is introduced as  $\lambda = np.poly1d(np.polyfit(x_{pix}, \lambda(x_{pix}), 1))$ , such that for any given pixel array ( $array_{pix}$ ) its associated wavelengths can be obtained ( $\lambda(array_{pix})$ ). On the other hand, from the color maps of the lamps, both the angle of rotation of the images (since a small angle is introduced into the slit depending on how tightly the pieces fit together) and the size of the slit can be determined. From this size, the images can be cropped to make them as precise as possible.

## 2.3. Applying corrections for data reduction

Once the background noise, rotation angle and image size have been determined, the data for stars and nebulae are reduced. The order in which the data is manipulated is important in order not to lose information during the process.

### 2.3.1. Gain analysis

During data collection, a standard gain of 140 is set. However, in some of the measurements this value is modified in order to obtain more favorable results (if, for example, the star is dim, the exposure time and gain of the program are usually manipulated to obtain a more precise spectrum). This involves performing a small calibration calculation given by the following relationship:

$$G_P \cdot 0.1 = 20 \cdot \log_{10}(G_R) \quad (2)$$

where  $G_P$  is the program gain (modifiable depending on the astronomical object) and  $G_R$  the actual gain. Based on the  $G_P$  values employed for each object, the  $G_R$  associated can be determined and thus, evaluating the quotient between  $\frac{G_R(G_P)}{G_R(G_P=140)}$ , the images can be divided by this factor, thus establishing an equivalent gain ratio between all of them (see *Figure 6*). This process is carried out prior to noise reduction due to the fact that the “*Masters*”, a priori, present gain 140 and should not be corrected.

**Figure 6.** Example of gain correction for the first Orion data stream. Analogous procedure for the rest of the astronomical objects.

```

1 # Nebulosa de Orión (Orion_1 y Orion_2 representan la franja superior de la nebulosa a tiempos de exposición
2 # diferentes. Orion_3, en cambio, representa la franja inferior en la que se detecta no solo nebulosa sino
3 # estrella).
4 path_orion1 = 'NEBULOSAS/ORION/Orion_1/23_45_24/*.fits'           # texp_ORION_1=30s (5 imágenes)
5 Lista_orion1 = glob.glob(path_orion1)                                     # GANANCIA = 510
6 orion1_array = np.zeros((len(Lista_orion1),3520,4656))
7 for i in np.arange(len(Lista_orion1)):
8     hdu_01 = fits.open(Lista_orion1[i])
9     orion1_array[i] = hdu_01[0].data
10 orion1_ruido = orion1_array / 70.82

```

### 2.3.2. Image reduction, rotation and cropping

The noise is then removed from the images to obtain what is known as a “*science image*”, given by:

$$Imagen_{ciencia}(t_{exp.}) = \frac{Imagen_{Ruido}(t_{exp.}) - Master Bias - Master Dark(t_{exp.})}{Master Flat} \quad (3)$$

It is important to mention that, just as the relation (1) was used for times outside the range of “*Master Darks*”, it can be seen from *Figure 7* that, from the array of times used for the experimental “*Darks*” and their corresponding associated “*Master Darks*” (section 2.1.2.), an interpolation relation is established that allows, from a given time within this range, to determine its associated “*Master Dark*”.

**Figure 7.** Interpolation function to obtain “*Master Darks*” with exposure times within the established range.

```

1 # Se define la función de interpolación:
2 t_exp = np.array([2, 20, 40, 60])
3 MasterDarks = np.array([MD_2s, MD_20s, MD_40s, MD_1min])
4 f_interp = scipy.interpolate.interp1d(t_exp, MasterDarks, bounds_error = False, axis = 0)

```

Finally, the images are rotated by the appropriate angle to keep them straight and cropped to set the slit region that will provide the information needed by the rest of the code (see *Figure 8*).

**Figure 8.** Final reduction of the first string of data from Orion.

```

1 # Orion 1 (texp=30s):
2 orion1 = np.zeros((len(Lista_orion1), 820, 4696))
3 o1 = np.zeros((len(Lista_orion1), 3520, 4656))
4 for i in np.arange(len(Lista_orion1)):
5     o1[i] = (orion1_ruido[i] - MB - f_interp([30])) / MF
6     orion1[i] = ndimage.rotate(o1[i], 0.6593)[1325:2145,:]

```

*Figure 8* also shows that the last string of data has dimensions 4696 x 820 precisely because of the rotation and cropping step (if the opposite had been done, the dimensions would be different and information would have been lost). It should also be noted that the images are currently only cropped along the “counts” axis (y axis), keeping the length of the pixel array invariant so as not to remove relevant information.

## 2.4. Wavelength calibration of stellar spectra and subtraction of the sky contribution

Once the image strings of each star are obtained, already reduced and ready to be manipulated, the first step is to choose the one that presents the most suitable spectrum for each case. Once selected, it is represented as counts versus wavelengths, based on the relationship shown in section 2.2. These results (see figure 9 (A)) would be referring to the stellar spectra with the contribution of the sky, present in the slit. It should be noted that, in particular for the star HD-176896, negative counts are observed, which does not fit with physical predictions. After an analysis it was observed that perhaps the program itself did not fit well with the gain analysis detailed in section 2.3.1, and a different relationship from (2) may be necessary. However, no viable solutions were found, so the analysis is continued with the data in the same way.

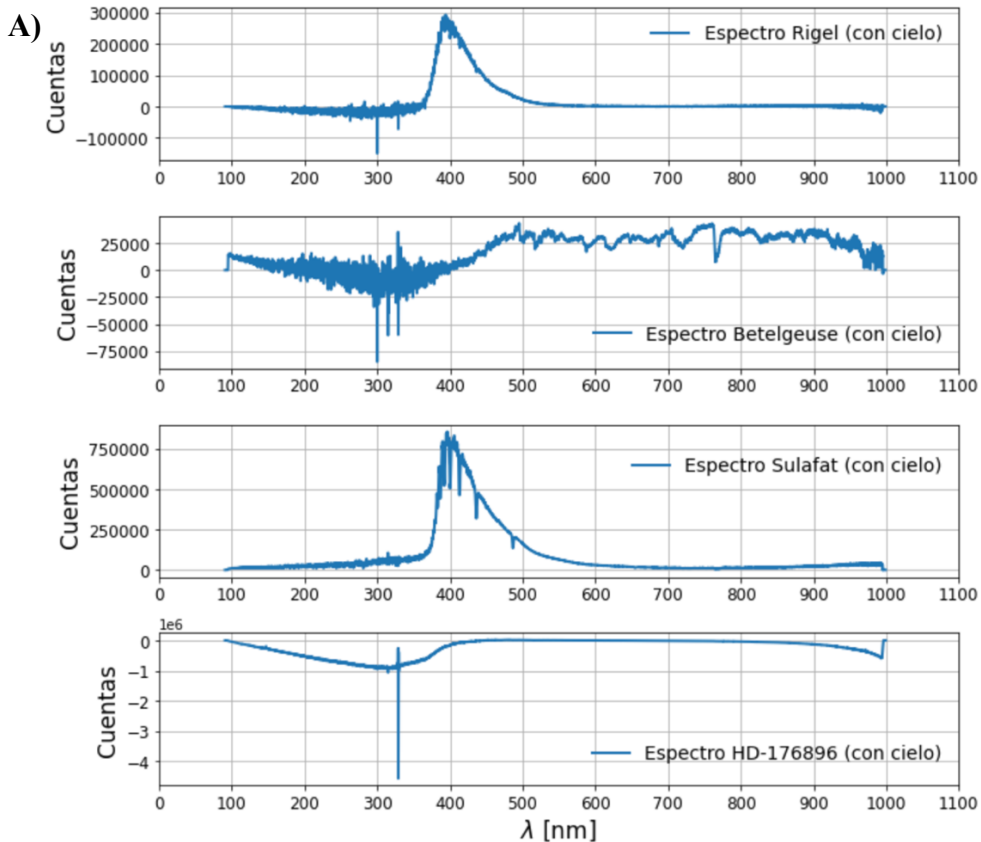
The next objective is to subtract the sky contribution from the images to obtain spectra where the stars are represented in their entirety. To do this, from the color maps of each one of them, the area where the star is located is cut out. On the other hand, the regions of the sky are cut out and the following relation is applied:

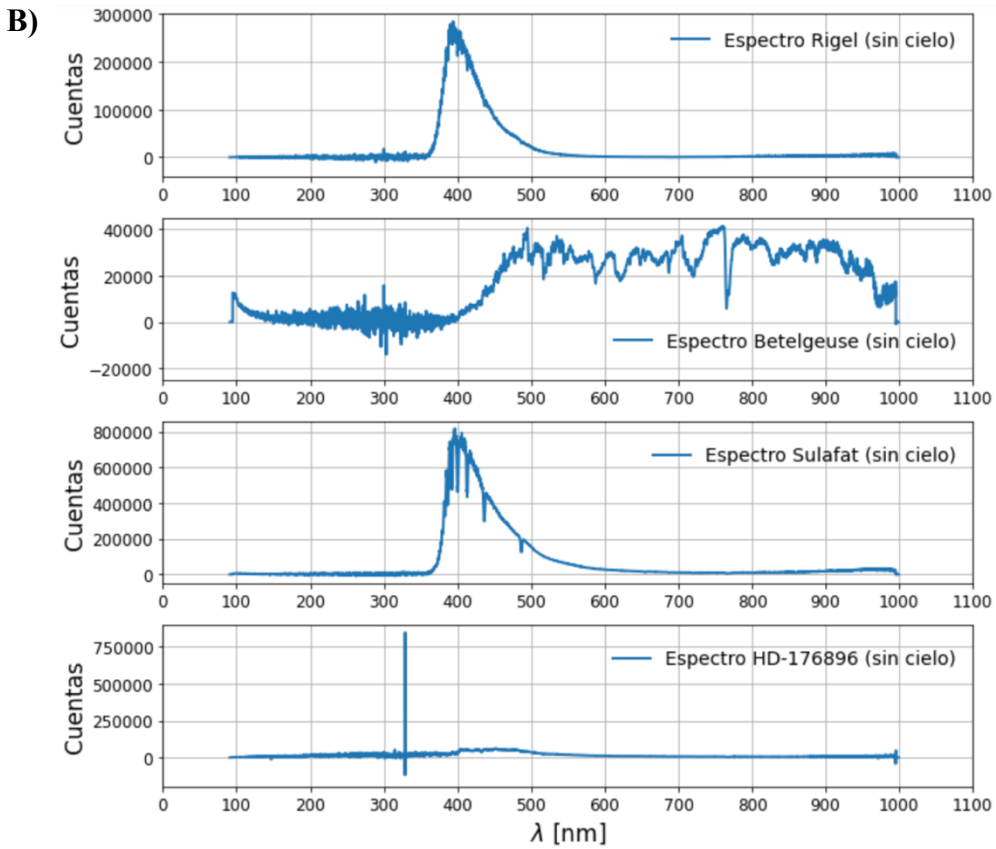
$$Espectro_{Final} = Espectro_{Comp.}^* - \mathcal{F} \cdot \left( \sum_{i=1}^{\# secciones\ de\ cielo} Espectro_{Comp.}^{C i-\text{ésimo}} \right) \quad (4)$$

where  $Espectro_{Comp.}^*$  refers to the section of the compressed star (its cropped and compressed spectrum),  $Espectro_{Comp.}^{C i-\text{ésimo}}$  is the spectrum of the  $i$ -th section of the sky once compressed and  $\mathcal{F}$  is a multiplicative factor which depends on the width of each cropped section,  $\mathcal{F} = \frac{\Delta^*}{\sum_i^{\# secciones\ de\ cielo} \Delta_i^{Cielo}}$ , where  $\Delta$  refers to the selected widths. Proceeding as indicated, the final spectra of the stars are obtained (see *Figure 9 (B)*).

In addition to the clear difference in the spectra after the sky subtraction, it can be seen that the stars Rigel and Sulafat are blue (B8Iae and B9III) while Betelgeuse is red (M1-M2Ia-lab). HD-176896, on the other hand, presents peculiarities that are analyzed in *section 2.5* because at first glance its spectral type could not be identified, even though theoretically it should be a red star (K0III). It is worth highlighting the presence of absorption lines, characteristic of stellar spectra.

**Figure 9.** Comparison of stellar spectra with and without sky contribution.





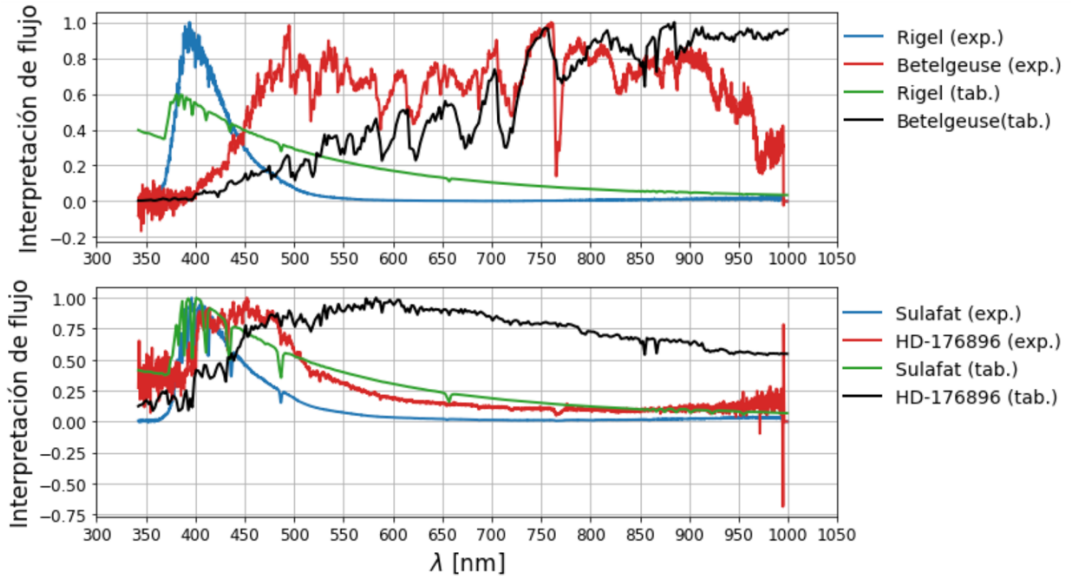
## 2.5. Flux calibration of stellar spectra and instrumental response curve

Next, it is necessary to perform a conversion of counts to flow units, which will allow the spectra of the objects to be represented appropriately. For this purpose, archival data are used.<sup>[4]</sup>, choosing the spectra associated with each star based on its temperature, radius, surface gravity and parallax<sup>[5, 6]</sup>. Once determined (and making a small calculation required by the conditions of use) the library spectra are “adjusted” to the resolution of the experimental spectra so that they can be represented in the same graph. This is achieved with the interpolation function, in which, from the experimental wavelengths and the flow data and tabulated wavelengths, the corresponding readjusted file flow is returned.

$$\text{Flujo}_{\text{reajustado}}^{\text{tab.}} = \text{np.interp}(\lambda_{\text{exp.}}, \lambda_{\text{tab}}, \text{Flujo}_{\text{tab.}}) \quad (5)$$

All the spectra are then normalized in order to be able to represent them in unison and make a more visual comparison. This means that the units on the y-axis are now more like “flow interpretations”. The spectra are then cut on the x-axis in order to select the region with the most information. In the case of the star HD-176896, it is first cropped and then normalized to avoid the influence of the pixel in  $\sim 8,33 \cdot 10^5$ .

**Figure 10.** Representation of the experimental spectra of the stars with respect to the tabulated ones.



From *Figure 10* it is verified that, indeed, Rigel and Sulafat are blue stars while Betelgeuse is red, all of them with a well-characterized spectrum with respect to the tabulated values. However, in the case of HD-176896 a discrepancy with respect to the archived spectrum is found, verifying that in reality a neighboring star with a blue spectral region was measured (it is believed that during the calibration problem with the program during the observation either HD-176913 or HD-177109 was detected).

It is determined below what is known as the “*instrumental response curve*” (IRC) which is a relationship between the experimental and tabulated spectra and is characteristic not only of the calibration stars used to generate it but also of the instrumental apparatus used. The main objective is to develop the curve between Rigel and Betelgeuse and compare it with that of Sulafat and HD-176896 but, since the latter turned out to be blue, curves are drawn for each star (omitting HD-176896) to check their disparities.

The relationship necessary for the creation of the curve is the one represented in *Figure 11*, in which the spectra are cut as was done previously and the experimental ones are divided by their exposure time in order to obtain “Counts/s/Flow” units for the curves. Since they are not homogeneous (see *Figure 13*), a Gaussian filter is applied to each of them, they are normalized and a convolution function is created with it, which is necessary to be able to smooth them and obtain the instrumental response curves for each star.

**Figure 11.** Example of the Rigel instrumental response curve construction code.

```

1 # Curva de respuesta instrumental: RIGEL
2 CRI_r = (espec_rigel[1300:]/1.5) / FLUJO_r[1300:]
```

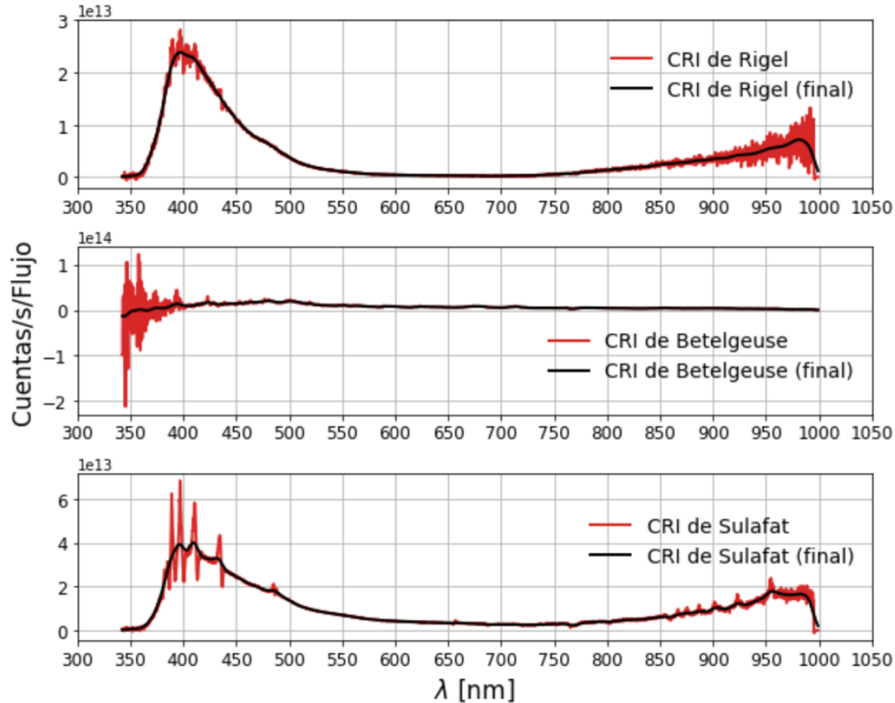
**Figure 12.** Example code for smoothing the Rigel instrumental response curve.

```

1 gaus_r = signal.gaussian(len(CRI_r), 20) # el 20 sale de la anchura de los picos (aprox)
2 gaus_norm_r = gaus_r/np.nansum(gaus_r) # "nansum" pues se requiere un área bajo la curva
3 # de valor 1
4 curva_r = np.convolve(CRI_r, gaus_norm_r, mode='same')

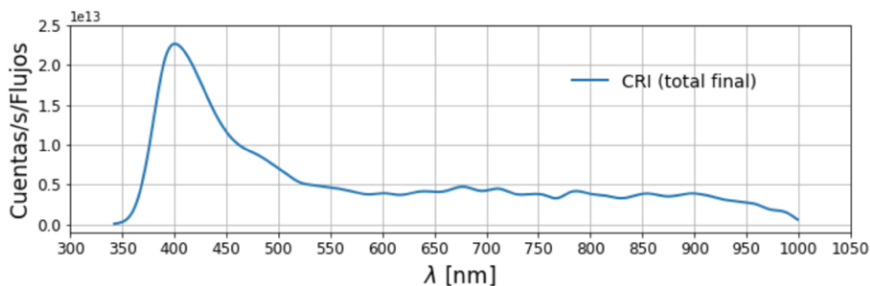
```

**Figure 13.** Representation of the initial response curves and after applying their Gaussian adjustments.



The response curve is shown to differ depending on whether the star is red or blue, which is why calibration stars belonging to opposite spectral ranges are often chosen when constructing the curve. Also, comparing Rigel with Sulafat, it can be seen that, despite the fact that both are blue, the resolution for each is slightly different. (~10% error). This occurs because Sulafat spent more time inside the slit compared to Rigel, resulting in a somewhat lower flux for the latter. Therefore, the total instrumental response curve associated with the sum of Rigel and Betelgeuse is developed, which is used in the rest of the study.

**Figure 14.** Final total instrumental response curve.



## 2.6. Calibration of nebula wavelengths

The next step is to convert pixels to wavelengths for the analysis of nebulae. The procedure is somewhat analogous to that used for stars in section 2.4, except for certain peculiarities implied by the fact that we are now working with nebulae.

### 2.6.1. Orion Nebula

We start from the Orion Nebula, which is characterized by not only a gaseous region but also a star at the beginning of the slit, as can be seen in *Figure 15*. By representing its associated spectral zone, we obtain the color map in *Figure 16*, in which both the intensity of the star and the emission lines of the nebula can be effectively distinguished. Both images are associated (their interpretation is visually highlighted with red indicators).

**Figure 15.** Orion Nebula.

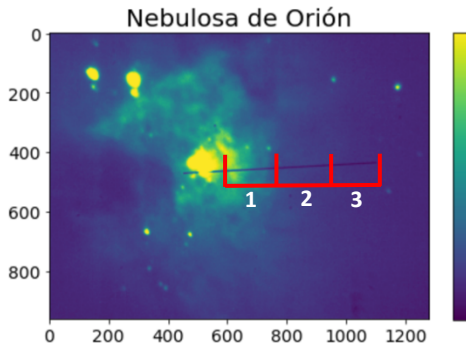
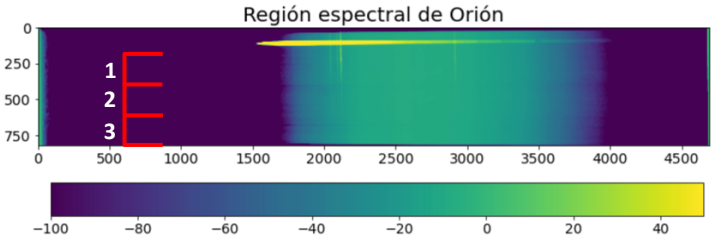


**Figure 16.** Spectral region of study (Orion).



The first step is to select equidistant fragments of the map, compress them and divide them by the exposure time of the astronomical object, again, to establish units of “Counts/s”. In this case, the sky is not subtracted since the slit only collects nebula (the dark area is still dense gas, it is not sky). It can also be observed that the region with the star is omitted since the current interest is in determining the emission lines of the nebula itself and the presence of the star could distort the results. The calibration is then carried out in wavelengths, obtaining for each of the regions spectra in units of “Counts/s” versus wavelengths.

### 2.6.2. Ring Nebula

In the case of the Ring Nebula, its complete map could not be measured as was the case with Orion, however, its appearance resembled a circular gas region with a hole in the centre (see *Figure 17*) where the intensity decreased. Its spectral zone, therefore, was a region of sky combined with alternating strong and weak emission lines as observed in figure 18. Similarly to the previous case, four sections are selected: the sky, a first bright region, a dark zone and a second bright region. Each of them is compressed and, applying in this case the relation (4), the contribution of the sky to the three remaining regions is subtracted (since in this case the slit does not only capture the nebula). Finally, spectra are obtained again in units of “Counts/s” versus wavelengths for each section.

**Figure 17.** Ring Nebula<sup>[7]</sup>.

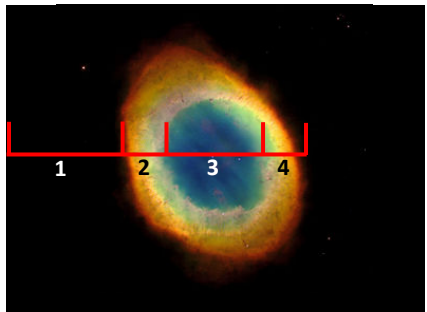
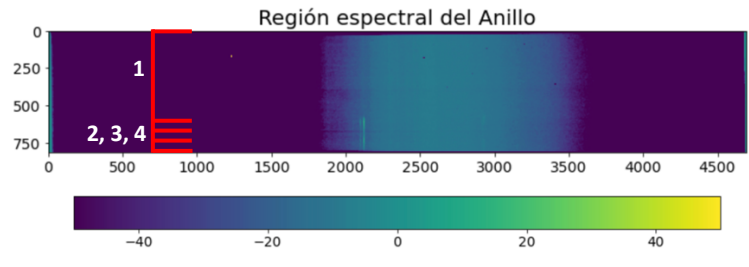


**Figure 18.** Spectral region of study (Ring).

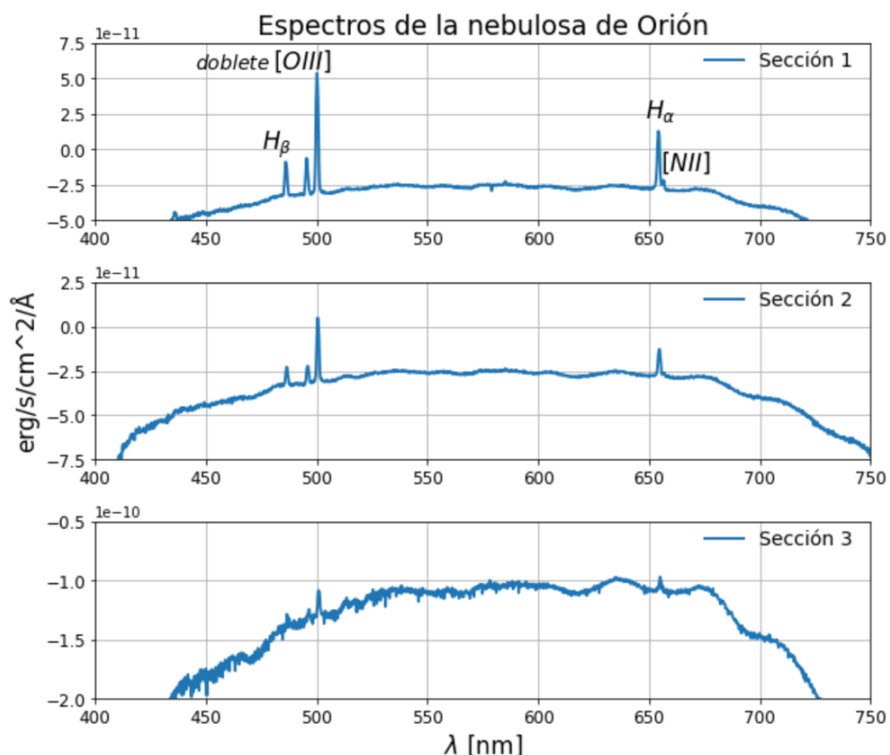


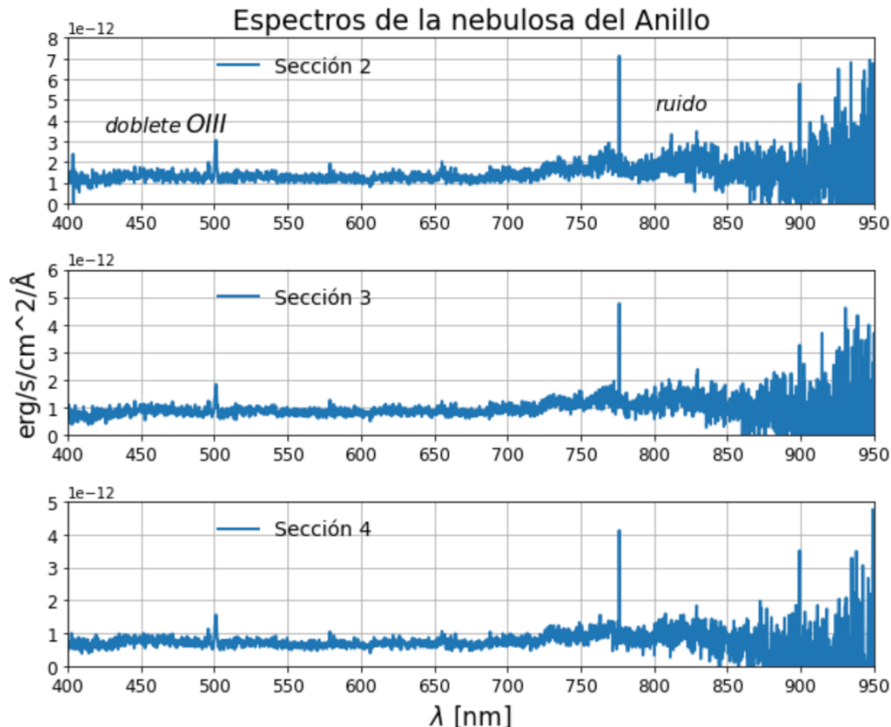
## 2.7. Generation of nebula spectra from the instrumental response curve

From the spectral regions determined in section 2.6, the instrumental response curve (see *Figure 14*) is applied using the relationship detailed in *Figure 11*, in order to determine their corresponding spectra in physical units of “erg/s/cm<sup>2</sup>/Å” versus wavelengths. It should be remembered that, when applying the curve, the spectral regions of the clipped nebulae must be used, since according to *Figure 11* the curve was developed from clipped spectra of calibration stars.

From *Figure 19* the main emission spectral lines detected for each nebula can be determined.

**Figure 19.** Spectra of selected regions for each nebula.





For the Orion Nebula, it is possible to distinguish mainly the emission lines of the hydrogen spectrum,  $H_\alpha$  and  $H_\beta$  (associated with  $\lambda_{tab.}(H_\alpha) = 656,3\text{nm}$  and  $\lambda_{tab.}(H_\beta) = 486,1\text{nm}$ ), the twice-ionized oxygen doublet  $[OIII]$  (with  $\lambda_{tab.}^{(1)}([OIII]) = 495,9\text{nm}$  and  $\lambda_{tab.}^{(2)}([OIII]) = 500,7\text{nm}$ ) and nitrogen singly ionized  $[NII]$  ( $\lambda_{tab.}([NII]) = 658,3\text{nm}$ ). It can be observed that, as a section is represented further and further away from the area of the lines (according to *Figure 16*) emission peaks are detected that are less and less intense and defined, until reaching a “continuum”. It is worth highlighting the difference between allowed lines ( $H_\alpha$  and  $H_\beta$ ) and forbidden lines ( $[OIII]$  and  $[NII]$ ), where the first occur as a consequence of the recombination of the atom and the second occur due to the collision of free electrons against atoms, ionizing them and giving the corresponding transitions (these occur only at low densities). <sup>[8, 9]</sup>.

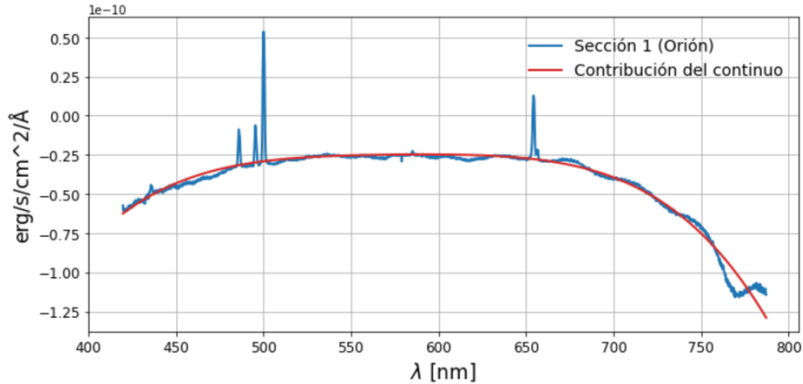
On the other hand, the spectra of the Ring Nebula are observed. In this case, only the twice-ionized oxygen doublet can be distinguished because the object presents saturation in the spectrum due to an overexposure error. This is why there is a predominance of noise, clearly identifiable in the graphs. However, it can be verified that the spectral intensity detected is greater for the first bright section, decreasing for the dark area and remaining approximately unchanged in the last region.

## 2.8. Continuum removal and representation of the final spectra of nebulae

To conclude the study, the continuous contribution to the spectrum is eliminated, which sometimes reduces information when analyzing the results obtained. The procedure is based on

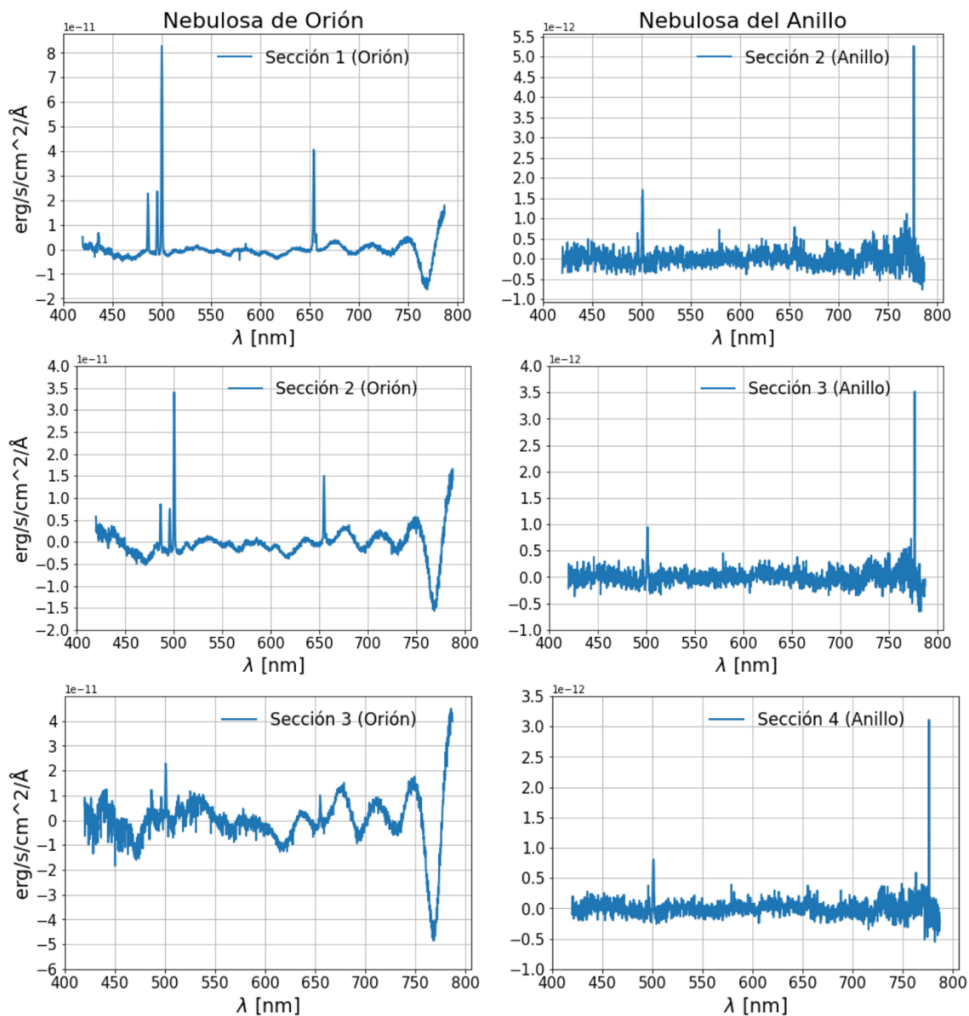
the spectra in *Figure 19*, generating for each of them a fit to a fourth-order polynomial, a procedure analogous to that carried out for the linear fit in *Figure 5*.

**Figure 20.** Continuum contribution to the first section of the Orion spectrum (example).



It would be enough to subtract this contribution from the total spectrum to obtain the final results. *Figure 21* shows these results for each section of the nebula, now showing spectra with fewer negative counts but with the same essential information as those represented in *Figure 19*.

**Figure 21.** Final spectra of nebulae.



### 3. Conclusions

During the study, data reduction codes were initially developed in order to eliminate the background noise present in the information collected after the observation. Then, and from the elaboration of mercury and neon lamp spectra, not only the calibration ratio of pixels to wavelengths was determined but also the rotation angle of the images and the precise width of the slit. By applying all these contributions to the raw results obtained and attributing to the analysis a function for the gain (which, far from finding another more suitable for the instrument, was assumed to be viable), the science images for the stars and nebulae were obtained.

Next, the stellar spectra, essential for the calibration in flux, were analyzed by creating the instrumental response curve. Initially, the spectra were calibrated in wavelengths and their contributions were subtracted from the sky. Later, tabulated spectra were obtained for the same stars in order to compare the quality of the measured data and observe the importance of evaluating stars with different spectra. It was also possible to verify that the star HD-176896 was actually blue and after an analysis of the individual response curves, the one corresponding to the sum of Rigel and Betelgeuse was obtained, the latter showing a much broader spectral range and applied to the rest of the study.

Continuing with the analysis, the nebula spectra were calibrated to wavelengths, but not before making sections of them and analyzing them as separate spectra, subtracting or not the sky depending on the case of study. Next, the instrumental response curve was applied to each section, thus obtaining the nebula spectra in physical units of flux versus wavelengths and verifying the presence of emission lines, which are characteristic of nebulae and less visible in the case of the Ring due to an oversaturation in the measured data. Finally, by subtracting the continuum contribution from each spectrum, the final results of the observational spectroscopy study were extracted.

Throughout the process, negative regions were detected in the spectra, results that go against the physical predictions that indicate the need for purely positive flows. After checking both the data reduction code and the analysis code, the discrepancy was attributed to a possible inappropriate use of the gain function, which is appropriate for maximum values of 300 when the experimental setup allows values of up to 600. Nevertheless, the results seem to fall within the theoretically established range and it is possible to determine spectral lines characteristic of low-density media such as nebulae.

## 4. References

- [1] JV Díaz, «Spectroscopy» Universo Blog, [Online]. Available: <https://josevicentediaz.com/astronomia-practica/espectroscopia/>
- [2] Daniel, «Flats» Dastronomía, 21 August 2008. [Online]. Available: <http://www.dastronomia.com/505/flats/>
- [3] «Typical Spectra of Oriel Instruments Spectral Calibration Lamps»
- [4] «CASTELLI AND KURUCZ ATLAS» Space Telescope Science Institute (STScI), [Online]. Available: <https://www.stsci.edu/hst/instrumentation/reference-data-for-calibration-and-tools/astronomical-catalogs/castelli-and-kurucz-atlas>
- [5] F. Chereau and G. Chereau, «Stellarium Web» [Online]. Available: <https://stellarium-web.org/>
- [6] «SIMBAD: basic query» University of Strasbourg/CNRS, [Online]. Available: <https://simbad.unistra.fr/simbad/sim-fbasic>
- [7] «Ring Nebula» Wikipedia, the free encyclopedia, 2 Oct 2022. [Online]. Available: [https://en.wikipedia.org/wiki/Ring\\_Nebula](https://en.wikipedia.org/wiki/Ring_Nebula)
- [8] A. R. López Sánchez, «The barcode of nebulae» Universo Rayado, 27 Nov 2015. [Online]. Available: <https://universorayado.naukas.com/2015/11/27/el-codigo-de-barras-de-las-nebulosas/>
- [9] CE Tapia Ayuga, «Emission lines» From A to CETA, [Online]. Available: [http://carlostapia.es/astro/lineas\\_emision.html](http://carlostapia.es/astro/lineas_emision.html)